Supporting Information

for

Visualisation of adjuvant penetration into plant waxes by fluorescence of Nile Red

Petr S. Sherin,[1] Michelle Wong Chap Lan,[1] Nicholas J. Brooks,[1] Markus Rueckel,[2] Marina K. Kuimova[1]

[1] Chemistry Department, Imperial College London, 82 Wood Lane, W12 0BZ, London, UK

[2] BASF SE, Carl-Bosch-Strasse 38, Ludwigshafen am Rhein, 67056, Germany

* Corresponding authors:

p.sherin@imperial.ac.uk,

markus.rueckel@basf.com,

m.kuimova@imperial.ac.uk

Table of Contents	**Page**

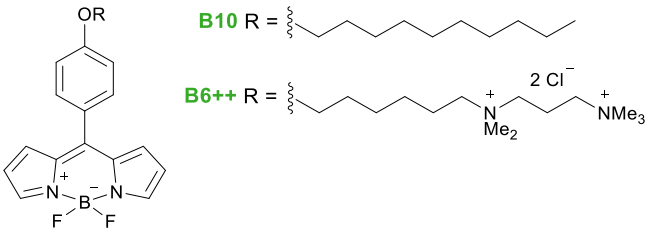

Chart S1. Chemical structures of BODIPY-based molecular rotors used to visualise the amorphous and crystalline phases of plant waxes, B10 and B6++, respectively. [1]

Colocalisation analysis

The quantitative colocalisation analysis is best suited to two images with discrete punctuate staining.[2] In the case of diffuse staining, the interpretation of Pearson's correlation coefficient (PCC) and distributions in the scatter plots is less straightforward. The photon noise is generally considered the main source of uncertainty in the quantitative analysis of confocal images.

In this work, we used median filtering to improve the signal-to-noise ratio. The PCC values were calculated for raw images and a consecutive increase in the dimension of median filtering from 3x3 to 15x15 pixels (Table S1). The scatter plots of intensities in two channels, BODIPY-based molecular rotors and NR (cyan and magenta in Figure 2of the main text), are given in Figure S1 for data processed with median filtering 3x3 and 9x9.

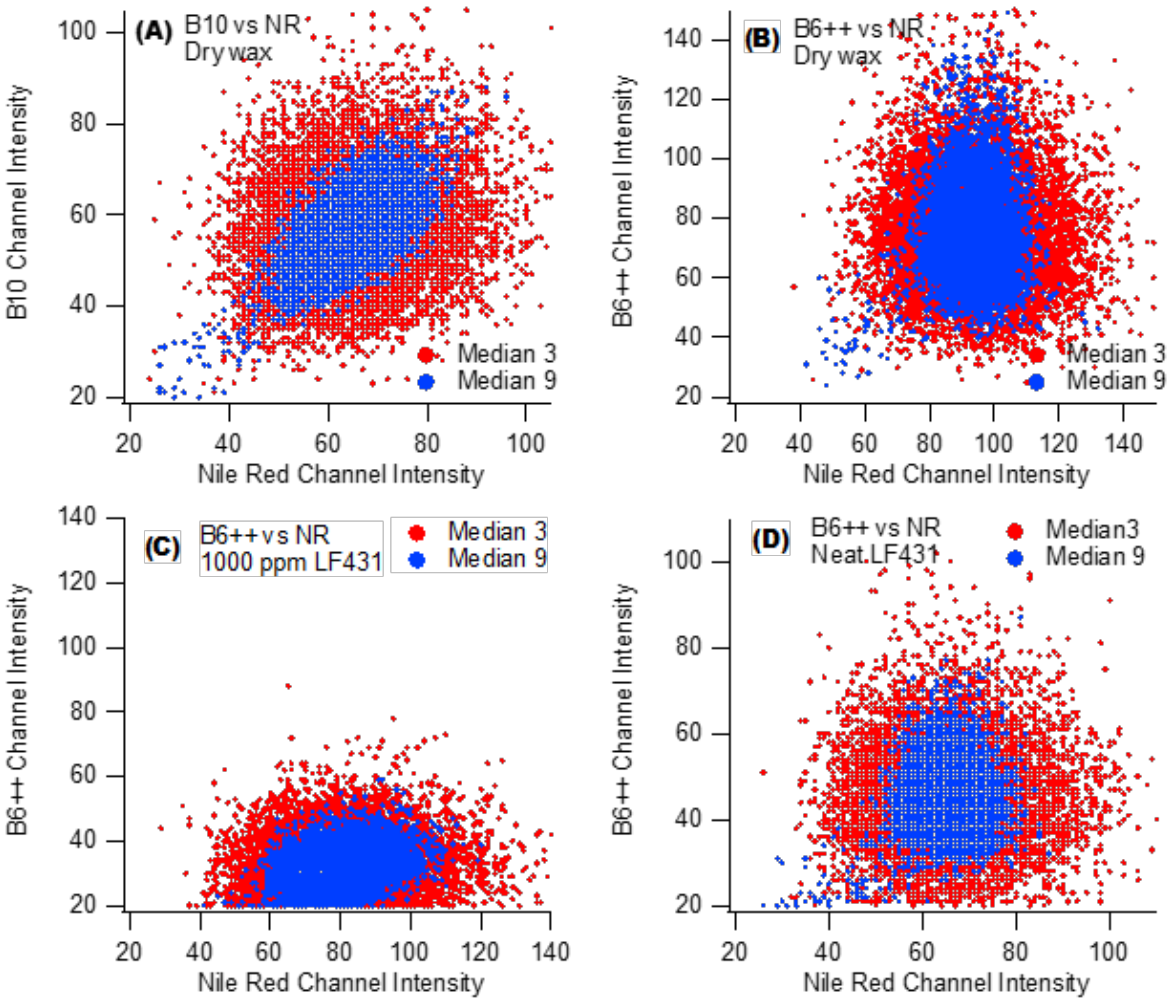

Figure S1. Scatterplots of pixel intensities in two channels corresponding to BODIPY-based molecular rotors (B10 or B6++, 'green' channel, 500-550 nm) and Nile Red (NR, 'red' channel, 580-650 nm). Data are shown for confocal images after the median filtering with the dimensions 3x3 (red points) and 9x9 (blue points).

The PCC values significantly increase with the median filtering dimension, i.e. the noise reduction. However, the image quality improvement does not affect the observed trends: the largest PCC values were obtained for dyes located in the amorphous phase (B10 and NR) and the smallest ones for the dyes in different phases (B6++ in the crystalline and B10 in the amorphous phase). This is confirmed by the scatter plots, which demonstrate the linear dependence only in the case of dyes in the same amorphous phase (B10 and NR, Fig. S2A). Compared to the case of dry wax (B6++ and NR), the exposure to the adjuvant in the aqueous solution leads to qualitatively different patterns (Figure 2, main text) with somewhat increased PCC values due to a partial overlap of different patterns. The application of the neat adjuvant results in images almost identical to the dry wax (B6++ and NR, Fig. 2 (A2-C2) and (A4-C4)), with similar PCC values and distributions in scatter plots (Fig. S1).

Table S1. Pearson's correlation coefficients (PCCs) were calculated for confocal images given in Figure 2 (of the main text) as raw images and after median filtering using different dimensions from 3x3 to 15x15.

	Staining conditions	Pearson's correlation coefficient				
			Median dimension			
		RAW	3	7	9	15
B10 vs NR	dry	0.0304	0.1661	0.513	0.6318	0.8152
B6++ vs NR	dry	-0.0017	0.0005	0.0343	0.0597	0.1509
B6++ vs NR	LF431 (1000 ppm)	0.0177	0.0923	0.2608	0.3181	0.4314
B6++ vs NR	LF431 (neat)	-0.0006	0.0038	0.0607	0.1054	0.2572

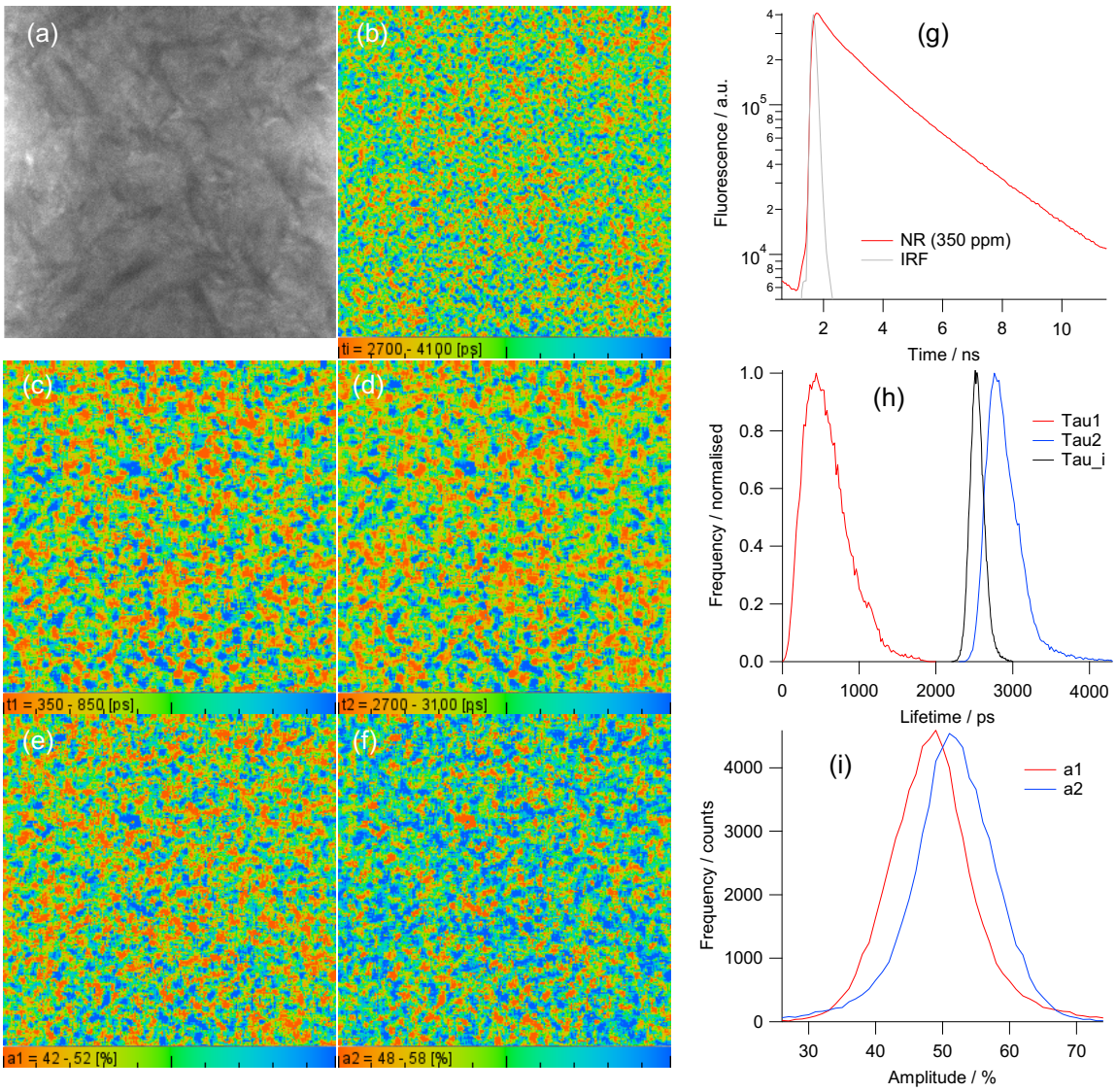

Figure S2. (a) Fluorescence intensity (black and white) and (b-f) FLIM (coloured) images recorded for Carnauba wax samples stained with 350 ppm NR. (g) Fluorescence decay trace averaged over the frame. (h) Distributions of lifetimes: the intensity-weighted average lifetime τ_i, and individual lifetimes τ_1 and τ_2, for datasets presented in (b), (c) and (d), respectively; (i) distributions of individual amplitudes a_1 and a_2 for datasets in (e) and (f), respectively, obtained from the two-exponential fit of FLIM data.

The index *i* means intensity-weighted average lifetime. The tau_i (τ_i) is defined as follows:

$$\tau_i = \frac{\sum_i A_i \times \tau_i^2}{\sum_i A_i \times \tau_i}$$

where A_i is the amplitude for i-component in the decay and τ_i is the corresponding lifetime.

The τ_i value was calculated for all biexponential decays, while annotation τ was used for the monoexponential decays.

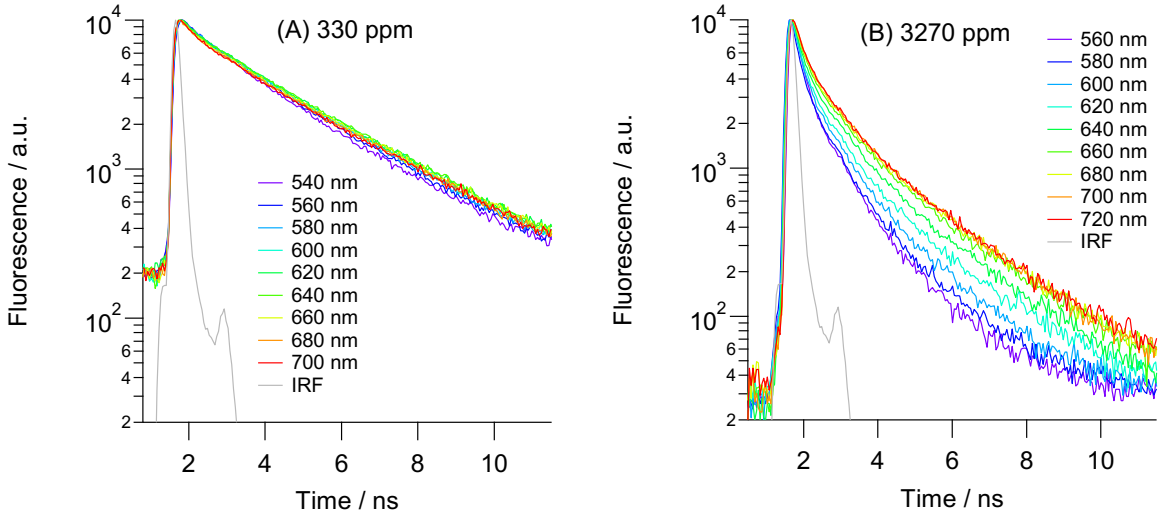

Figure S3. Fluorescence decay traces recorded with Carnauba wax samples stained with NR at (A) 330 ppm and (B) 3270 ppm at different wavelengths over the entire emission spectrum following the multiphoton excitation at 930 nm.

At low and moderate concentrations (40-500 ppm), NR exhibits almost wavelength-independent decays over the entire emission spectrum. In the case of high concentrations (> 500 ppm), the observed decays are wavelength dependent. However, no solvatochromic behaviour could be seen, i.e. no rise in the traces at the red edge of the emission band. This wavelength dependence originates from the reabsorption process due to high dye concentration, confirmed by changes in the emission spectra (secondary inner filter effect) (Figure S4).

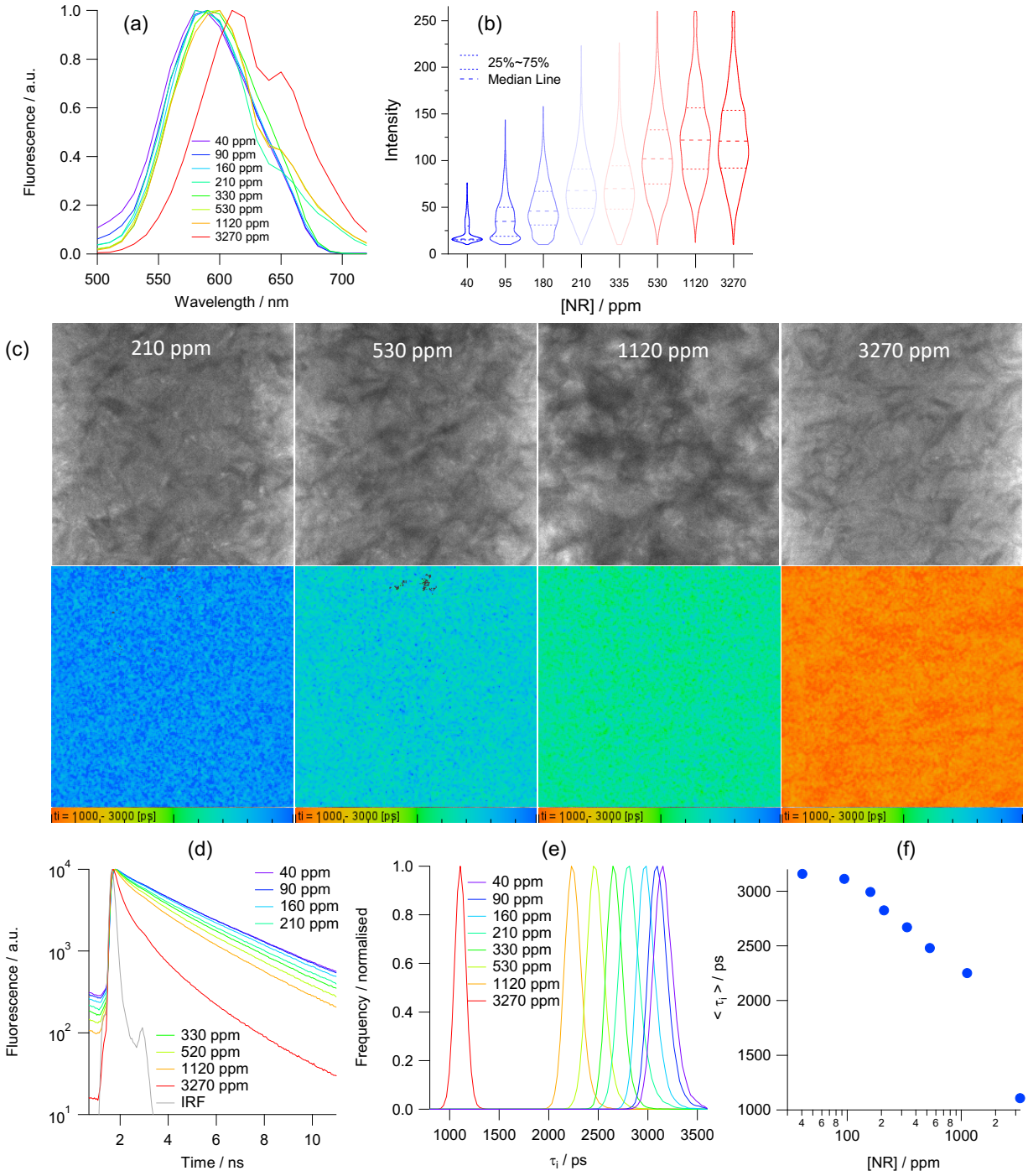

Figure S4. Carnauba wax samples stained with different concentrations of NR in the range of 40-3270 ppm; the data was obtained with dry samples following the multiphoton excitation at 930 nm. (a) Normalised fluorescence emission spectra. (b) Violin plots of intensity distributions in raw confocal images. Scale bars are 10 μm. (c) Fluorescence intensity (upper row) and FLIM (bottom row) images for selected NR concentrations. (d) Fluorescence decay traces averaged over FLIM frame. (e) Distributions of τ_i lifetimes. (f) Concentration dependence for the average τ_i lifetime.

We are not able to determine the arrangement of NR molecules in aggregates since any aggregation-induced shifts in the emission spectra are hidden by a large secondary inner filter effect (Figure S4a).

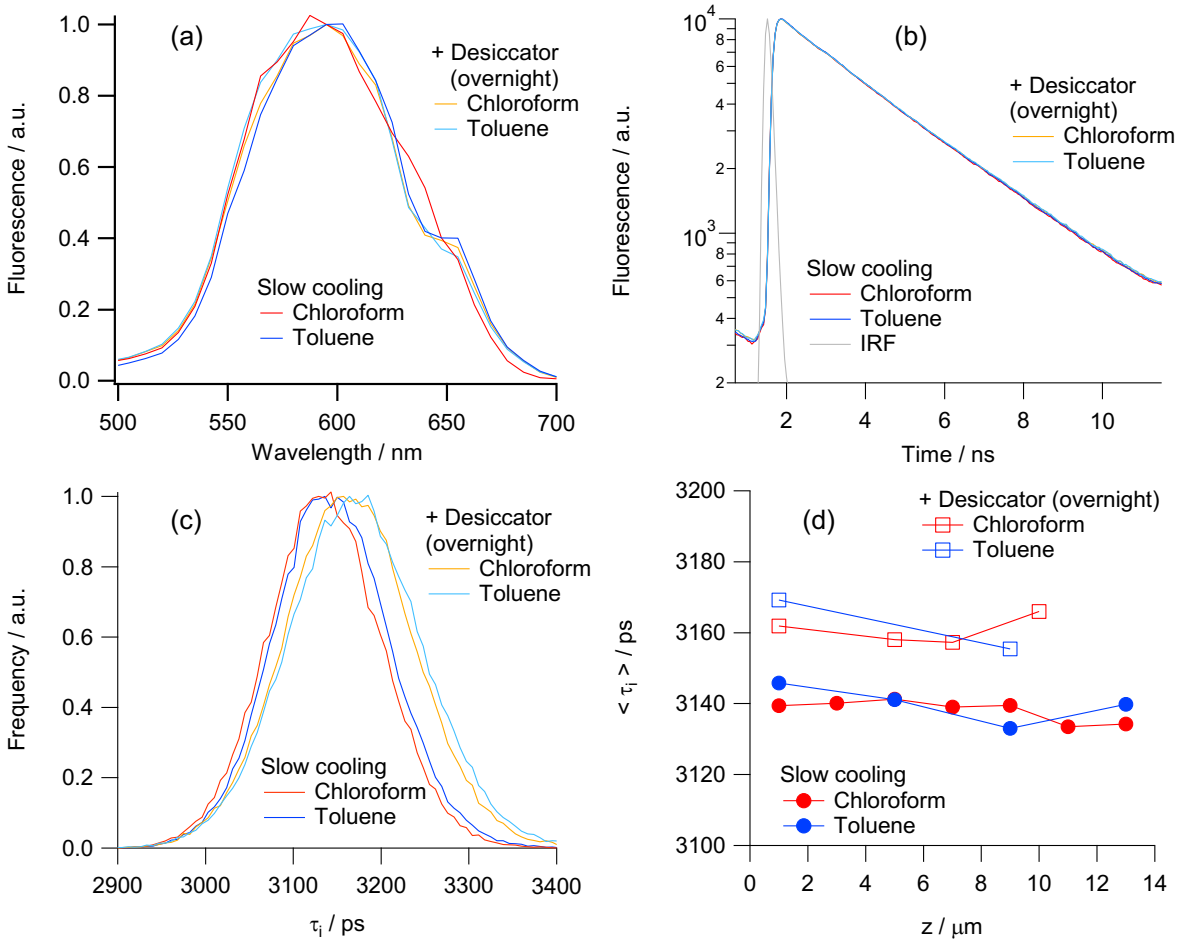

Figure S5. Carnauba wax samples stained with 210 ppm of NR via the wax dissolution in chloroform or toluene (after initial heating followed by slow cooling down), and additional overnight staining in the desiccator. Confocal and FLIM data were obtained following excitation at 930 nm and emission detection in 540-700 nm. (a) Normalised emission spectra. (b) Scaled fluorescence decay traces averaged over FLIM frames. (c) Normalised distributions of τ_i lifetimes. (d) Average τ_i lifetimes for different z positions within wax samples. Data in (a)-(c) are given for z = 1 μm.

Spectral and photophysical properties of Nile Red in bulk solvents

As the adjuvant Plurafac® LF431 induces a significant softening effect on the amorphous phase of Carnauba wax [1] and Nile Red (NR) is localised within the same phase, first, we hypothesised that the observed changes in τ_i value (Fig. 3f) could be related to viscosity variations. To verify this hypothesis, we measured the spectra and lifetimes of NR in a set of binary mixtures of toluene/castor oil, in which both components are of low polarities (ε = 2.4 and 4.7 for toluene and castor oil, respectively), close to Carnauba wax ($\varepsilon \approx 2.5$ at 20ºC [3]). Toluene/castor oil mixtures provided a large degree of viscosity variation within 0.5 – 920 cP [4]. The only visible change was a redshift in the NR emission maximum from 570 to 600 nm (Fig. S6a), passing from pure toluene to a mixture of 40% castor oil / 60% toluene due to the castor oil-induced dielectric constant increase up to $\varepsilon \approx 3.3$. Further variations in castor oil content resulted in negligible changes in the shapes of emission spectra (Fig. S6a) and lifetimes (app. 3.75 ns) over the whole range of used viscosities (Fig. S6b). Therefore, the viscosity is not responsible for the observed changes in τ_i value (Fig. 3 of the main text), and NR visualises other adjuvant-induced changes within the wax.

To verify the impact of ultra-low polarities and hydrogen bonds on NR spectral and photophysical properties, we performed the following experiments. First, ultra-low polarities were simulated with binary mixtures of n-pentane (ε = 1.85) and chloroform (ε = 4.81). In very low-polar media, NR exhibits several peaks in its emission spectrum, which correspond to the vibronic progression, as previously reported for other low-polar media as cyclohexane [5-7] and olefins [8]. The increase in polarity results in a monotonic redshift of the emission maximum from 520 to 600 nm and disappearance of vibronic progression (Fig. S6c). However, lifetime demonstrates another trend: a stepwise change of lifetime from 2.4 to 4.0 ns for a change ε from 1.85 to 2.0, followed by a slight increase of the τ value to 4.3 ns at ε > 2.0 (Figs. S6d and S6h). Note that the observed τ = 2.4 ns in non-polar n-pentane (ε = 1.85) is close to the τ_i value for the dry wax. However, the emission maximum is at 520 nm, which is too blue-shifted compared to the dry wax, which has a maximum at 600 nm (Fig. S6e). Therefore, within the wax, NR demonstrates spectra typical for low-polarity solvents (Fig. S6g), but with significantly shorter lifetime. It should be noted that NR emission from dry wax is closer to solvents with polarity around $\varepsilon \approx 4.8$ rather than solvents with polarity $\varepsilon \approx 2.5$, previously reported for Carnauba wax [3], which may indicate the location of NR in wax domains of higher polarity as compared to the value reported as an integral property of this natural wax.

Second, the emission spectra and decay traces were recorded with samples of NR in toluene in the presence of MeCN or MeOH (5 and 10%, v/v). Both MeCN and MeOH are highly polar solvents (ε = 37.5 and 32.7, respectively) with drastically different abilities to donate hydrogen bonds: MeCN is an aprotic solvent, while MeOH is a strong donor of intermolecular hydrogen bonds. The ability to donate a hydrogen bond could be characterised by a Kamlet-Taft parameter α, which is 0 for MeCN and 0.93 for MeOH [9]. The addition of MeCN or MeOH will provide an opportunity to separate the impact of polarity and hydrogen bonding on NR spectral and photophysical properties. The obtained results have shown a monotonic redshift of NR emission maximum with more pronounced effects of MeOH due to hydrogen bonds (Fig. S6e). However, these amounts of protic solvents

have a negligible impact on NR decay traces (Fig. S6f) and lifetimes (Fig. S6h). Therefore, the presence of low amounts of hydrogen bonding solvents (up to 10% by volume) in a low-polar solvent could be discriminated only by a shift of the emission band, but not the lifetime.

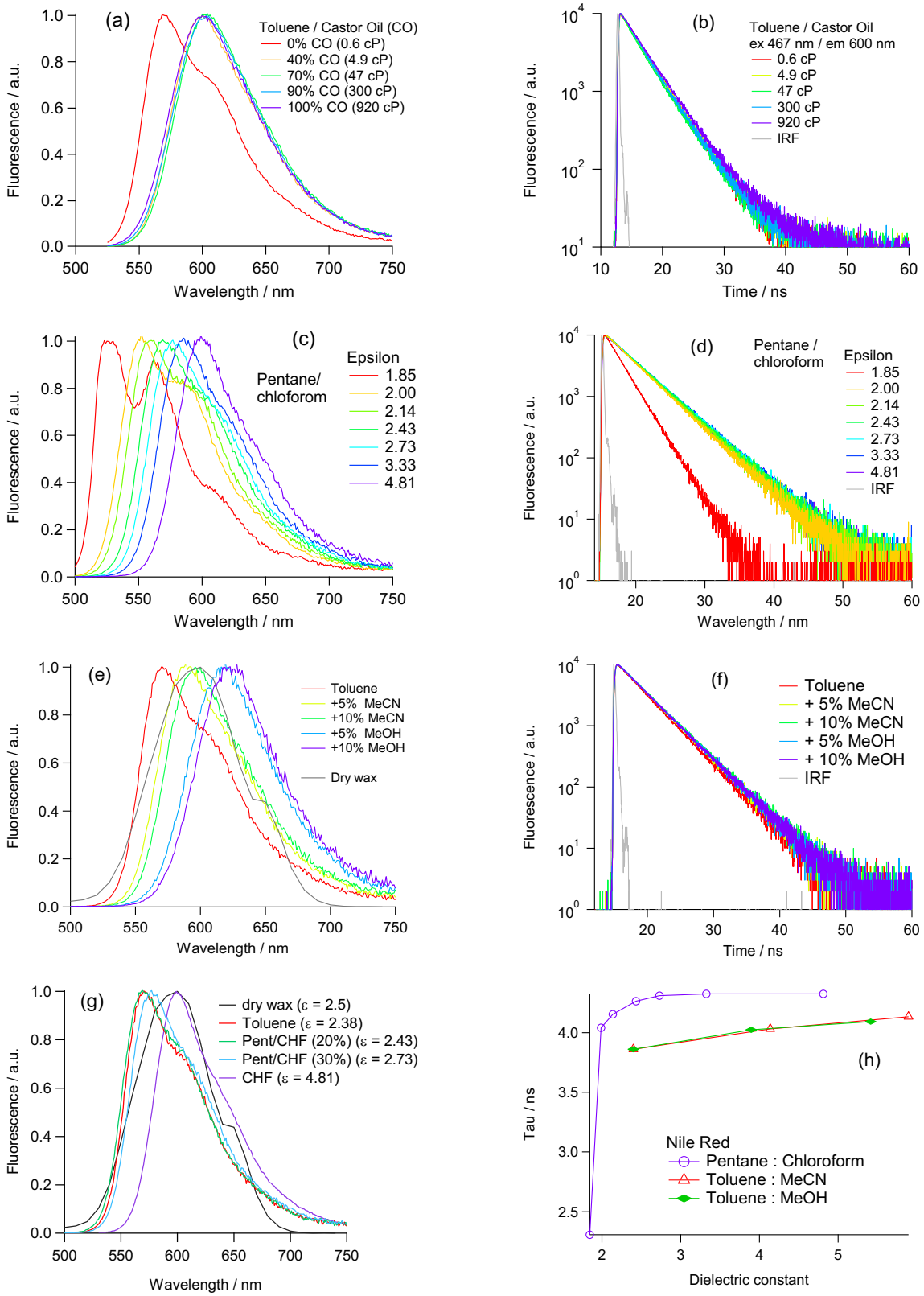

Figure S6. NR emission spectra (left) and fluorescence decay curves (right) recorded after the excitation at 467 nm and the detection at the emission maxima for the corresponding media. (a,b) NR in binary mixtures of toluene/castor oil; the mixture compositions and

corresponding viscosities [4] are given in legends. (c,d) NR in binary mixtures of n-pentane/chloroform; the mixture compositions and dielectric constants (ε), calculated as linear combinations of ε values for n-pentane (1.85) and chloroform (4.81), are given in legends. (e,f) NR in toluene with the addition of 5 and 10% (by volume) of MeCN or MeOH. Grey line: the emission spectrum of NR in Carnauba wax. (g) Comparison of emission spectra for NR in low-polarity solvents and Carnauba wax. (h) The dependence of τ (ε) obtained from the mono-exponential analysis of fluorescence decays in (d) and (f).

Quenching of Nile Red emission by Carnauba wax components

Carnauba wax is insoluble in chloroform at ambient temperature. We prepared several samples of wax of the same weight (10 mg) and different volumes of chloroform (80-250 μl). All samples were heated up to 50°C until the complete dissolution of wax with subsequent cooling down to the ambient temperature of 19°C. Samples with wax concentrations above the maximum solubility concentration (46 mg/ml) demonstrated precipitation of some wax components at room temperature. Samples with concentrations of 21 and 46 mg/ml were used for further measurements of spectral and lifetime measurements.

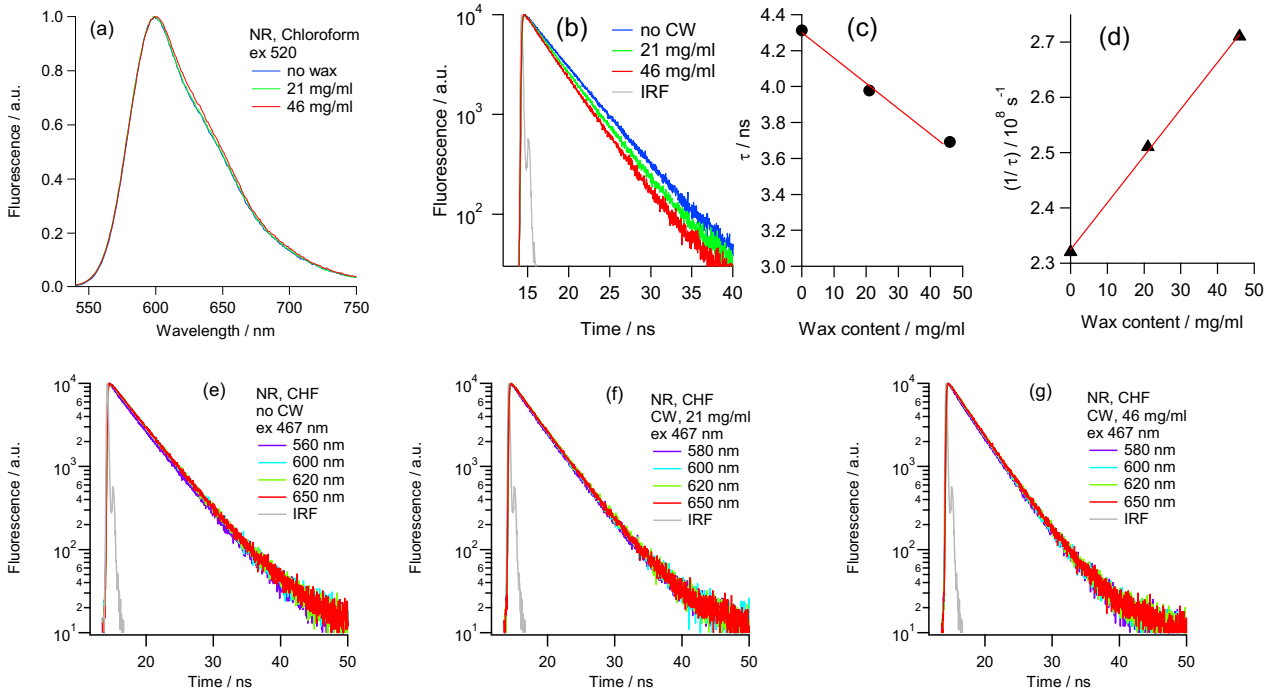

Figure S7. (a) Normalised fluorescence emission spectra and (b) fluorescence decay traces at 600 nm recorded with NR in chloroform in the absence and presence of Carnauba wax (CW). (c) NR lifetime and (d) the inverted lifetime dependences on the wax concentration. The red lines are the best linear fits. (e-g) Fluorescence decay traces recorded at different wavelengths over the whole emission band of NR in chloroform in the (e) absence and presence of CW with concentrations of (f) 21 and (g) 46 mg/ml. All emission spectra were obtained with the excitation at 520 nm, and decay traces at 467 nm.

Fluorescence lifetimes (τ) were obtained from monoexponential fits of decay traces in Fig. S7e-S7g. Linear approximation of $1/\tau$ vs C(wax), Fig. S7d, yields the rate constant (k_{CW}) of NR emission quenching as $k_{CW} = 8.9\times10^5$ $(mg/mol)^{-1}$ s^{-1}. Assuming that the average molecular weight of wax components is app. 700 g/mol, the k_{CW} could be estimated as 1.3×10^6 M^{-1} s^{-1}. This value should be considered a rough estimation because different classes of wax components quench the NR emission with different rate constants.

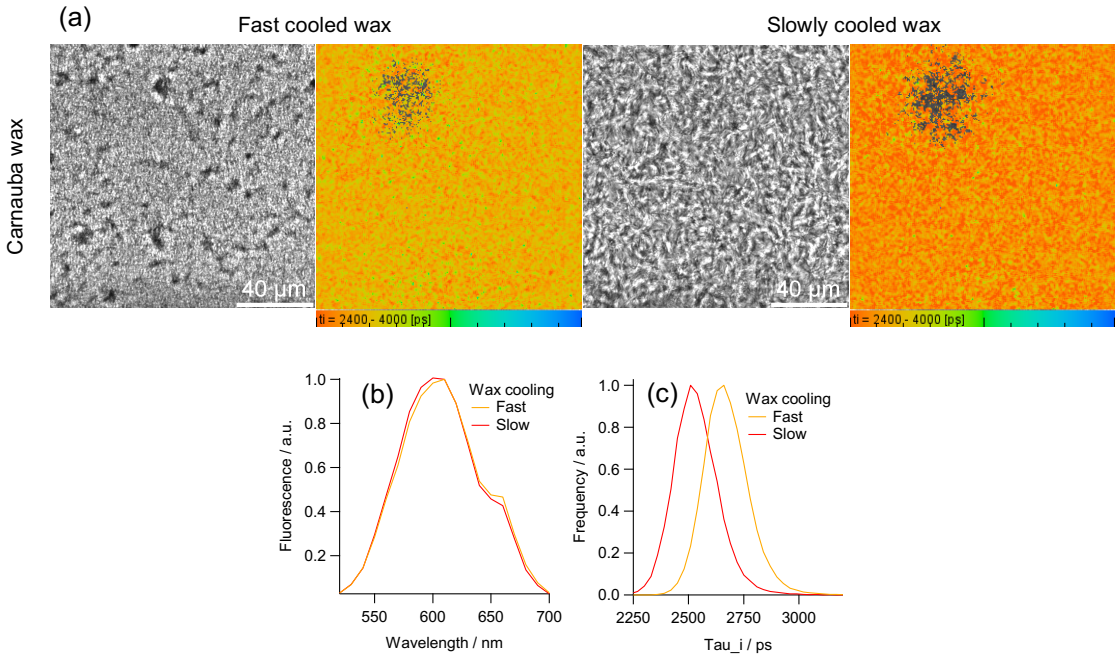

Fig. S8. (a) Fluorescence Intensity and FLIM images recorded with Carnauba wax samples stained with 330 ppm of Nile Red and cooled from 70 to 20 °C at different rates: a fast cooling within a few seconds and a slow cooling with a rate of 15°°C / 20 min. (b) Fluorescence spectra and (c) τ_i histograms obtained with samples presented in (a). All microscopy data were obtained after the excitation at 930 nm and detection in the range of 540-700 nm. Scale bars are 40 mm.

Quenching of Nile Red emission by lipids

To verify that the observed quenching of NR emission is a general feature of a lipid environment, we used three lipids, cholesterol (CL), egg yolk sphingomyelin (SM) and distearoylphosphatidylcholine (DSPC), and binary mixtures of CL/SM and CL/DSPC 1/1 (w/w) as simplified models of natural wax. Full datasets of transmission and FLIM images and their analysis are given in Figs. S9 and S10. Upon drying, the whole samples of each lipid form unified structures with ordered (CL, DSPC) or disordered (SM) morphologies, see Fig. S9-1. In each lipid, NR exhibits emission spectra close to those observed with dry Carnauba wax and lifetimes within the range of 3.4-3.6 ns (Fig. S10). Compared to bulk solvents of low polarity ($\tau \approx 4.0$-4.5 [5-7]), these lifetimes indicate quenching of NR emission by lipids independently of the lipid structure and the sample morphology. An aggregation of NR, as seen in the case of Carnauba wax (Fig. S4), could not be excluded and may contribute to some extent. However, the most interesting observations were obtained with samples of dried binary mixtures of lipids, which form at least two distinctly different structures with disordered and needle-like morphologies (Fig. S9-2). In the case of CL/SM mixture, NR demonstrates strictly different lifetimes of 4.1 and 3.4 ns for disordered and needle-like morphologies, respectively (Figs. S9-2 and S10). In the case of CL/DSPC mixtures, NR's lifetime within needle-like structures decreases down to 3.0-3.2 ns (Figs. S9-2 and S10), which are close to τ_i values obtained for the dry CW (Fig. 3f).

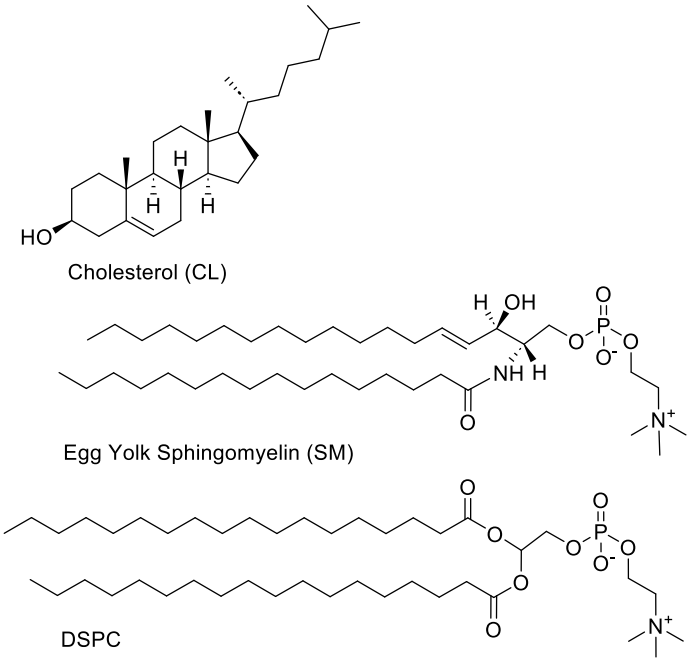

Chart S2. Chemical structures of used lipids: cholesterol (CL), egg yolk sphingomyelin (SM) and distearoylphosphatidylcholine (DSPC).

Two possible mechanisms of physical quenching should be discussed. First, a Forster Resonance Energy Transfer (FRET) from NR excited states to vibration modes of some wax components could be suggested according to the recent work on IR-emitting fluorescent dyes [10]. However, in our previous work [1], another red-emitting dye, a thiophene-based

molecular rotor, exhibited a decrease in lifetime upon adjuvant penetration, i.e. the effect opposite to that revealed by NR in this work. Therefore, FRET is unlikely to be responsible for the NR quenching within the wax.

The second mechanism could be energy dissipation via intermolecular hydrogen bonds between amino and carbonyl groups of NR (Chart 1) and some wax components, for instance, ω-hydroxy acid esters. This hydrogen bond-induced quenching of emission in bulk solvents of high proticity (alcohols and water) was previously reported for NR [7] and other charge transfer dyes [11-13], which typically exhibit significantly more pronounced quenching effects compared to NR. It should be noted that NR exhibits a redshifted emission maximum within the dry Carnauba wax compared to bulk solutions of similar dielectric constants (Fig. S6g). This shift may be considered as an indirect confirmation of hydrogen bonding interactions between NR and some of the wax components. We should emphasise that such interactions between NR and lipids should be confirmed in separate studies, which are out of the scope of this work.

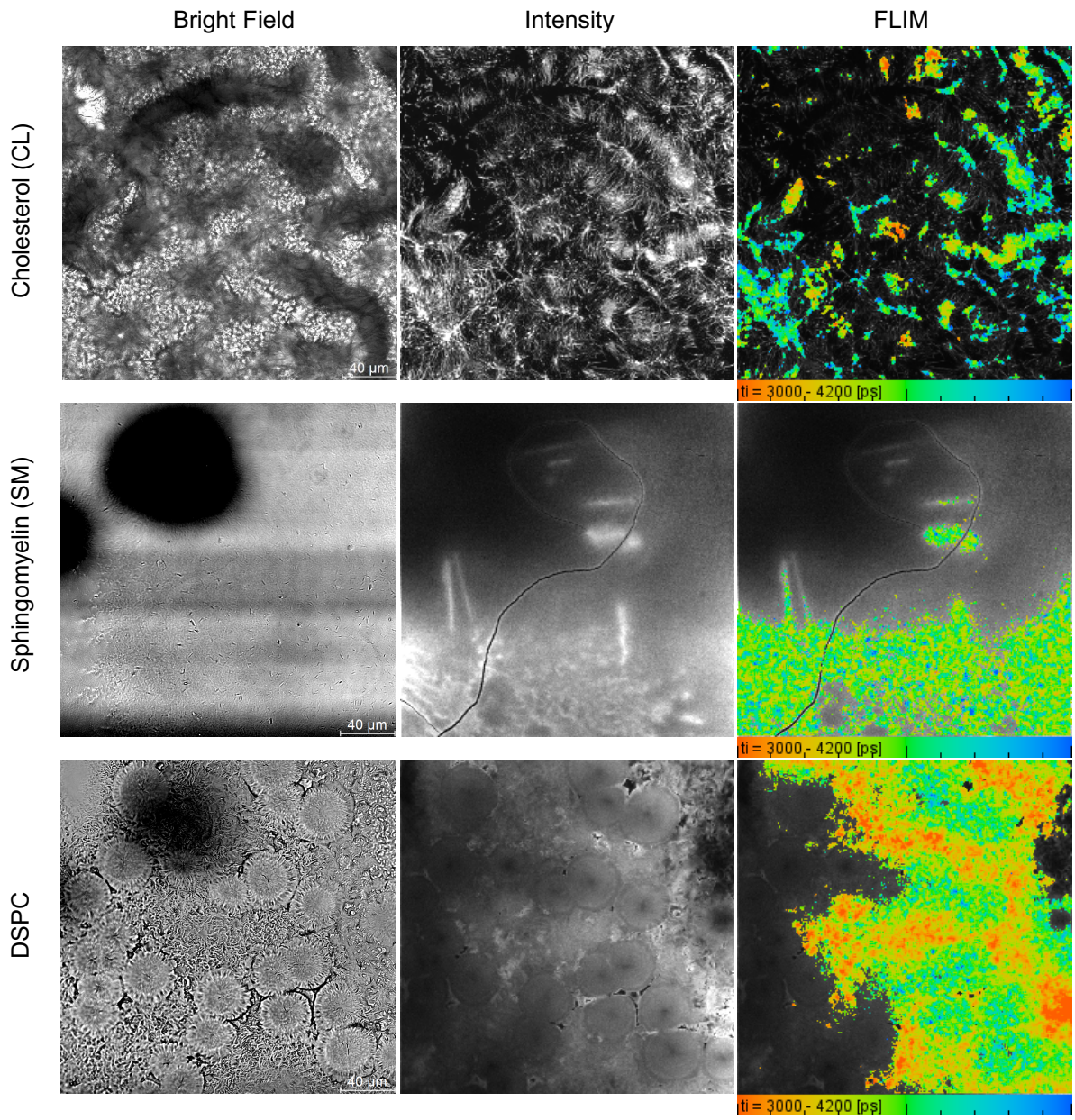

Figure S9-1. Transmission, fluorescence intensity (black and white) and FLIM (coloured) images recorded for lipid samples (described on the left) stained with 330 ppm NR. Images recorded following 930 nm excitation and 520-700 nm emission detection at the bottom of samples (see Figure 5c of the main text for the schematic presentation of the experiment). All data were recorded with the same x63 objective and (x1) magnification factor; the scale bar is 40 µm for all images.

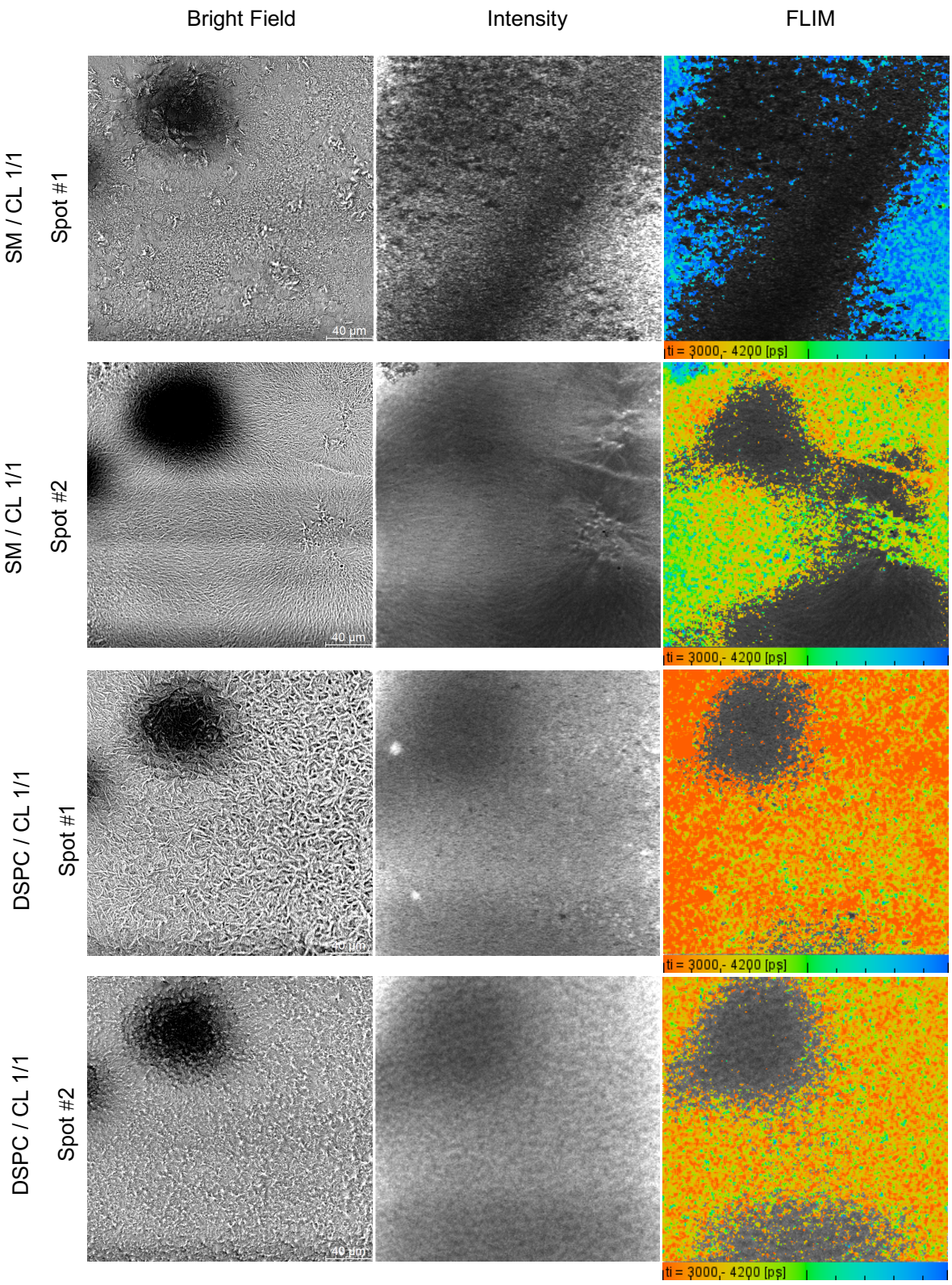

Figure S9-2. Transmission, fluorescence intensity (black and white) and FLIM (coloured) images recorded for lipid samples (described on the left) stained with 330 ppm NR. Images recorded following 930 nm excitation and 520-700 nm emission detection at the bottom of samples (see Figure 5c of the main text for the schematic presentation of the experiment). All data were recorded with the same x63 objective and (x1) magnification factor; the scale bar is 40 µm for all images.

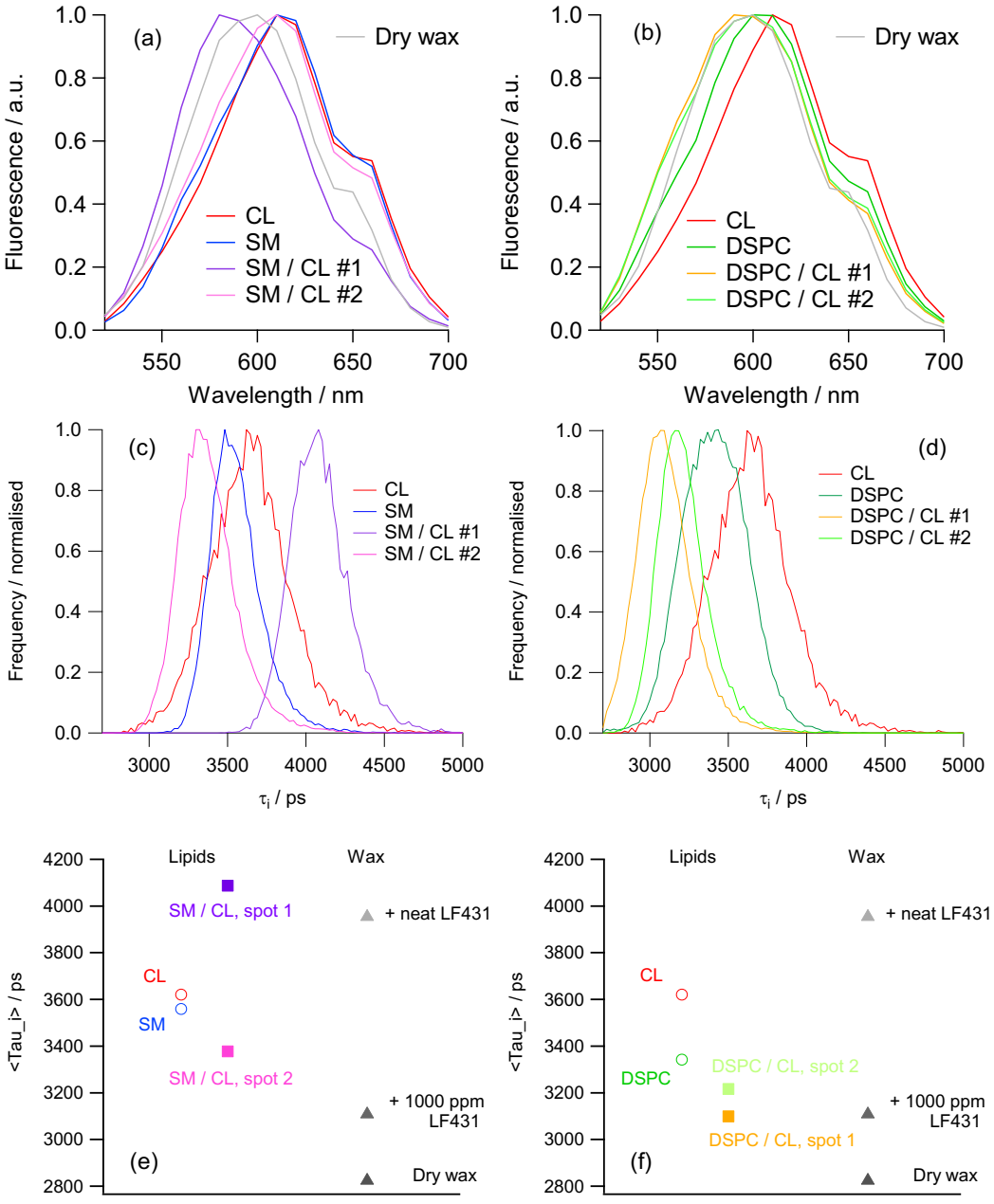

Figure S10. (a,b) NR emission spectra, (c,d) the τ_i distributions and (e,f) the averaged τ_i values (centres of gravity for histograms in (c,d)) obtained with samples of NR within dried lipids CL, SM and DSPC and binary mixtures of CL/SM and CL/DSPC at two different morphologies. The τ_i values for Carnauba wax samples under dry conditions and exposed to the aqueous solution, and the neat adjuvant Plurafac® LF431 (taken from Fig. 3f of the main text) are given in grey for comparison.

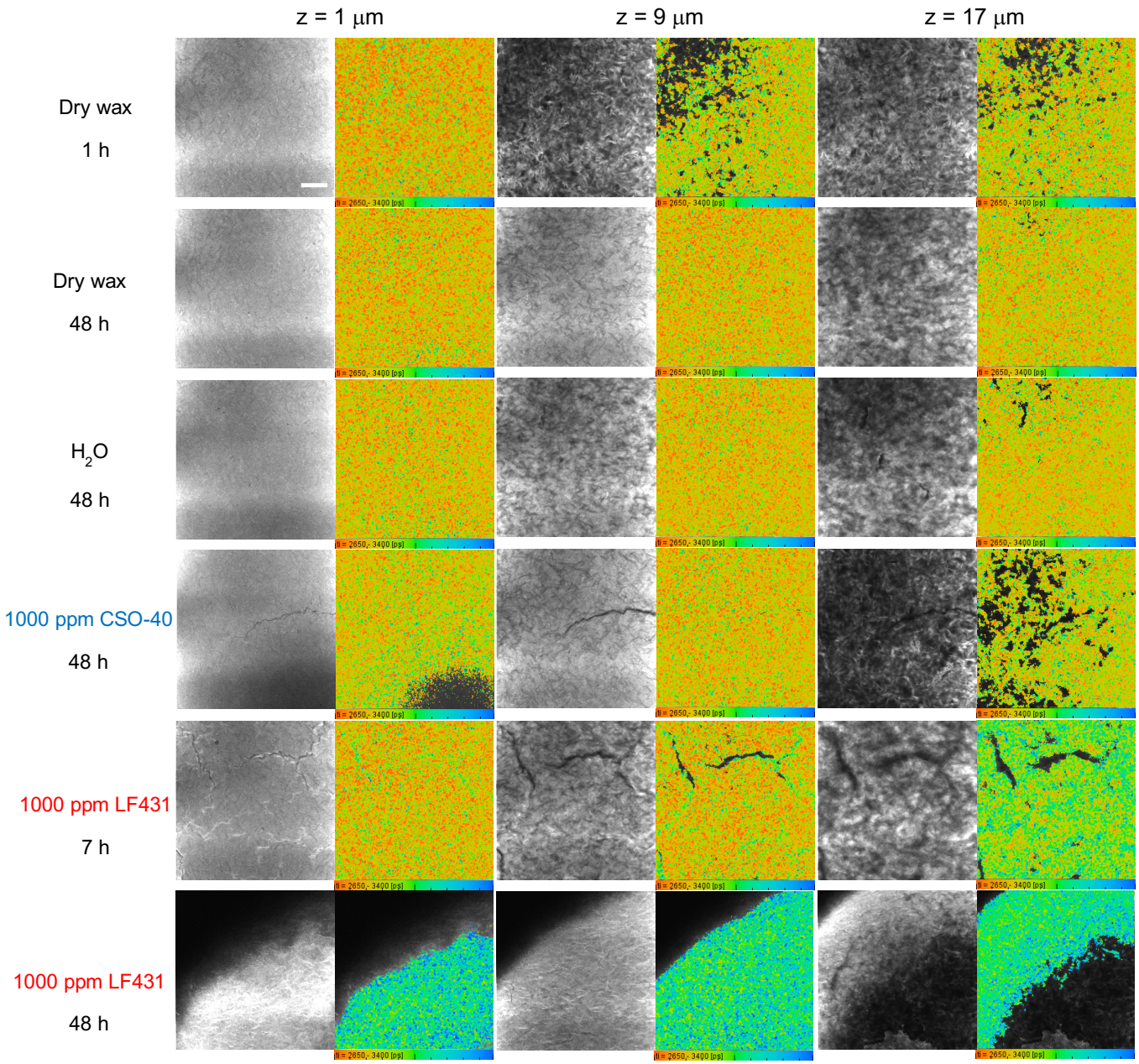

Figure S11. Fluorescence intensity (black and white) and FLIM (coloured) images recorded for Carnauba Wax samples stained with 330 ppm NR at different time intervals (1h, 7h and 48h) under four different conditions (described in the left column): dry, the exposure to aqueous solution in the absence (H_2O) and the presence of 1000 ppm of emulsifier (Agnique® CSO40) or adjuvant (Plurafac® LF431). Images recorded following 930 nm excitation and 540-700 nm emission detection at different z-positions within the wax layer, see Figure 5c of the main text for the schematic presentation of the experiment. All data were recorded with the same x63 objective and (x1) magnification factor; the scale bar is 40 μm for all images.

It should be noted that the adjuvant penetration inside the wax induces two unnatural morphological changes in the wax structure: the formation of cracks (Figs. 5b and S11) and wax buckling (Fig. S11) as was reported in our previous work [1]. We assign these effects to an increase in wax volume upon adjuvant dissolution within the wax, which, in turn, induces these morphological changes due to higher thicknesses of wax layers used in this work (12-20 μm) as compared to natural ones (< 2 μm [14]).

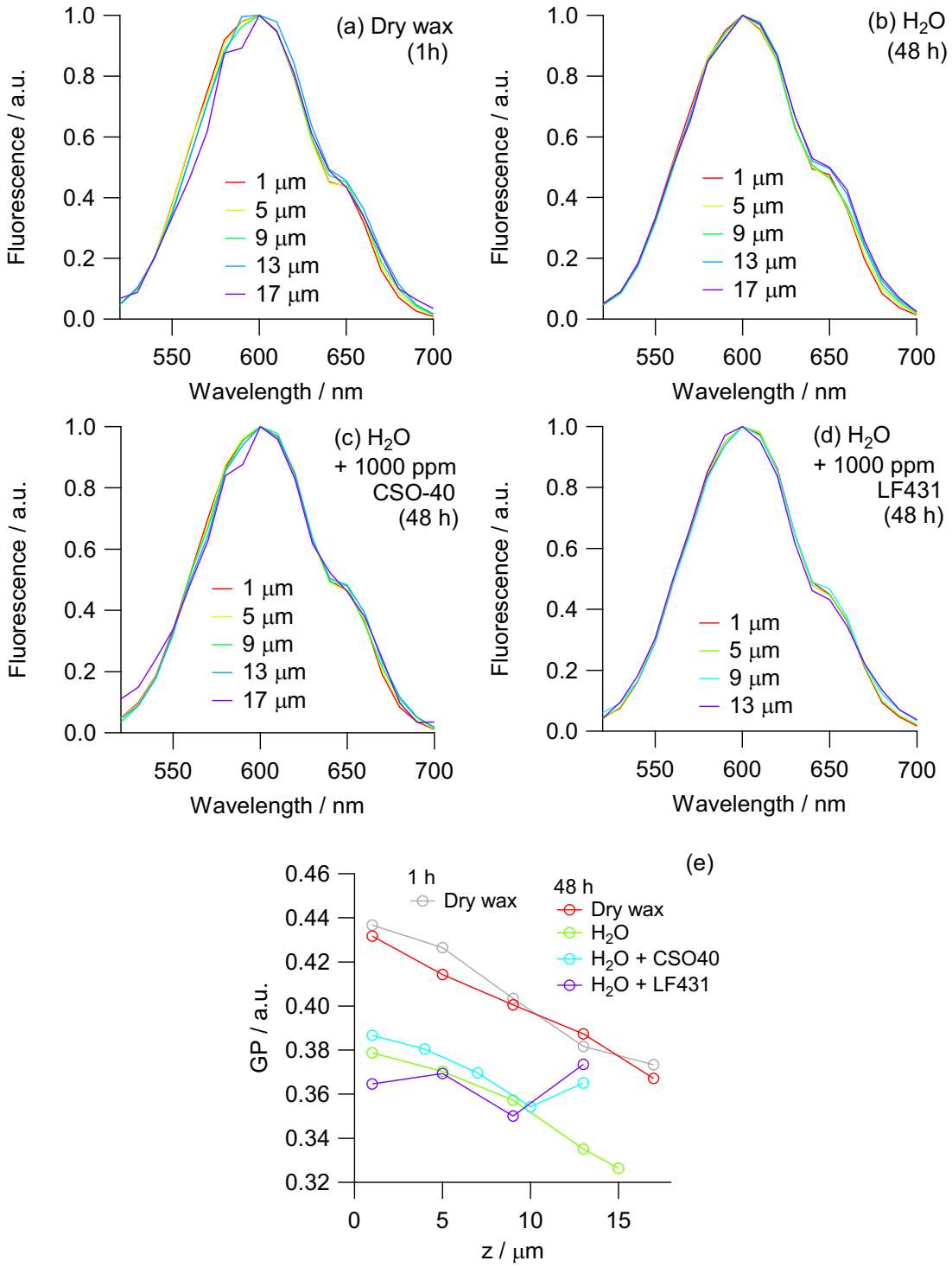

Figure S12. (a-d) Normalised fluorescence emission spectra recorded for Carnauba wax samples stained with 330 ppm NR at 48h under four different conditions: (a) dry, the exposure to aqueous solution in (b) the absence (H_2O) and the presence of (c) 1000 ppm of emulsifier (Agnique® CSO-40) or (d) adjuvant (Plurafac® LF431). Spectra recorded following 930 nm excitation without wavelength sensitivity correction at different z-positions within the wax layer, see Figure 5c of the main text for the schematic presentation of the experiment. All data were recorded with the same x63 objective and (x1) magnification factor. (e) z-Profiles of the Generalised Polarisation (GP) calculated from the spectra in (a-d) using the equation S1.

Generalised Polarisation (GP) of NR in CW is calculated according to the following equation:

$$GP(NR) = \frac{I_{520-620} - I_{620-700}}{I_{520-620} + I_{620-700}} \qquad \text{(S1)}$$

where $I_{520\text{-}620}$ and $I_{620\text{-}700}$ are areas of NR emission spectra for the wavelength regions 520-620 and 620-700 nm, respectively.

GP is used to quantify the changes in polarity within the lipid-rich media. A high GP is usually associated with low polarity and low fluidity, and a low GP is the opposite.

The following trends could be seen from the data obtained (Fig. S12e):

(i) A slight decrease in GP values along the z-axis within the dry wax layer;
(ii) Further decrease of GP values with the wax exposure to an aqueous solution;
(iii) No impact of the emulsifier Aqnique® CSO40 or adjuvant Plurafac® LF431.

Changes along the z-axis indicate a slight increase in the polarity and fluidity within the wax layer from the bottom to the top, which is exposed to ambient air. A modest decrease in GP values with the penetration of water inside wax points out a weak access of NR to water molecules within the wax. Most likely, these changes in GP values should be assigned to the penetration of water inside the wax, as was previously revealed by changes in lifetimes of molecular rotors [1].

It should be emphasised that the observed changes in GP values are close to or below the accuracy of the approach used. Thus, the trends revealed (Fig. S12e) should be investigated with an approach with higher spectral resolution and lower photodamage to the sample during data acquisition. The data presented should be considered as a demonstration of minor changes in polarity rather than a precise quantification of changes.

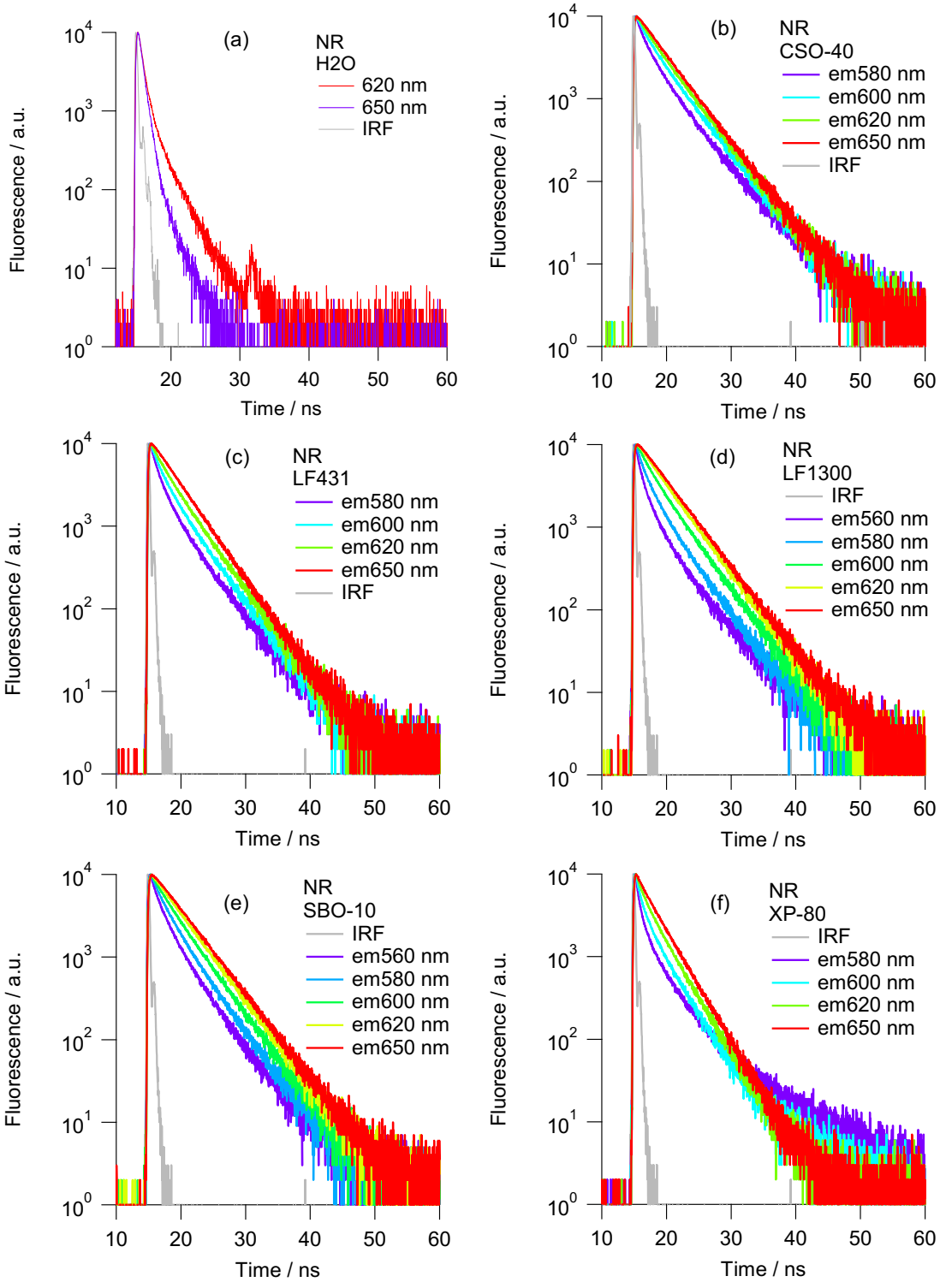

Figure S13. Fluorescence decay traces recorded at different wavelengths over the whole emission band of NR in aqueous solution in (a) the absence and the presence of (b) the emulsifier Agnique® CSO40 or the adjuvants (c) Plurafac® LF431, (d) Plurafac® LF1300, (e) Agnique® SBO10 and (f) Lutensol® XP80. All traces were obtained with the excitation at 467 nm.

It should be noted that NR demonstrates slow relaxation dynamics within all adjuvants that could be seen by a faster decay of NR emission at the blue side and a rise of signal at the red side of the emission spectrum (Fig. S13). This indicates a reorganisation of the adjuvant microenvironment around NR, which is highly polar in the excited states. The characteristic time constants for this relaxation dynamics were obtained in the global analysis of decay traces using a sum of two or three exponential functions; see the obtained values in Table S2.

Table S2. Characteristic time constants obtained from the global analysis of fluorescence decay traces from Figure S13 using a sum of three exponential functions. Lifetimes for NR in dry Carnauba wax sample, toluene, chloroform and the neat adjuvant are listed as τ_3 and given for comparison purposes.

Global analysis	Tau1 / ns	Tau2 / ns	Tau3 / ns
Dry wax	-	-	2.83
Toluene	-	-	3.86
Chloroform	-	-	4.32
Neat LF431	-	-	3.92
H_2O	-	-	0.54
+ 1000 ppm CSO40	0.98	-	4.21
+ 1000 ppm LF431	0.02	0.92	3.84
+ 1000 ppm LF1300	0.32	1.44	4.17
+1000 ppm SBO10	0.49	2.05	4.23
+ 1000 ppm XP80	0.47	-	3.06

Figure S14. A photo of Carnauba wax sample stained with 330 ppm NR after 72 h of exposure to the neat adjuvants (corresponding squares are labelled on the photo): Plurafac® LF431, Plurafac® LF1300, Agnique® SBO10 and Lutensol® XP80.

Table S3. Critical Micellar Concentrations (CMCs)* for agrochemicals used in this work.

Name of Chemical	Structure	CMC, mg/L (ppm)
Agnique® CSO40	castor oil ethoxylate	180
Plurafac® LF431	Guerbet alcohol alkoxylate methyl ether	4.2
Plurafac®LF1300	fatty alcohol ethoxylate	50
Agnique® SBO10	soybean oil ethoxylate	90
Lutensol® XP80	Guerbet alcohol alkoxylate	540

* CMC values were measured by BASF (unpublished).

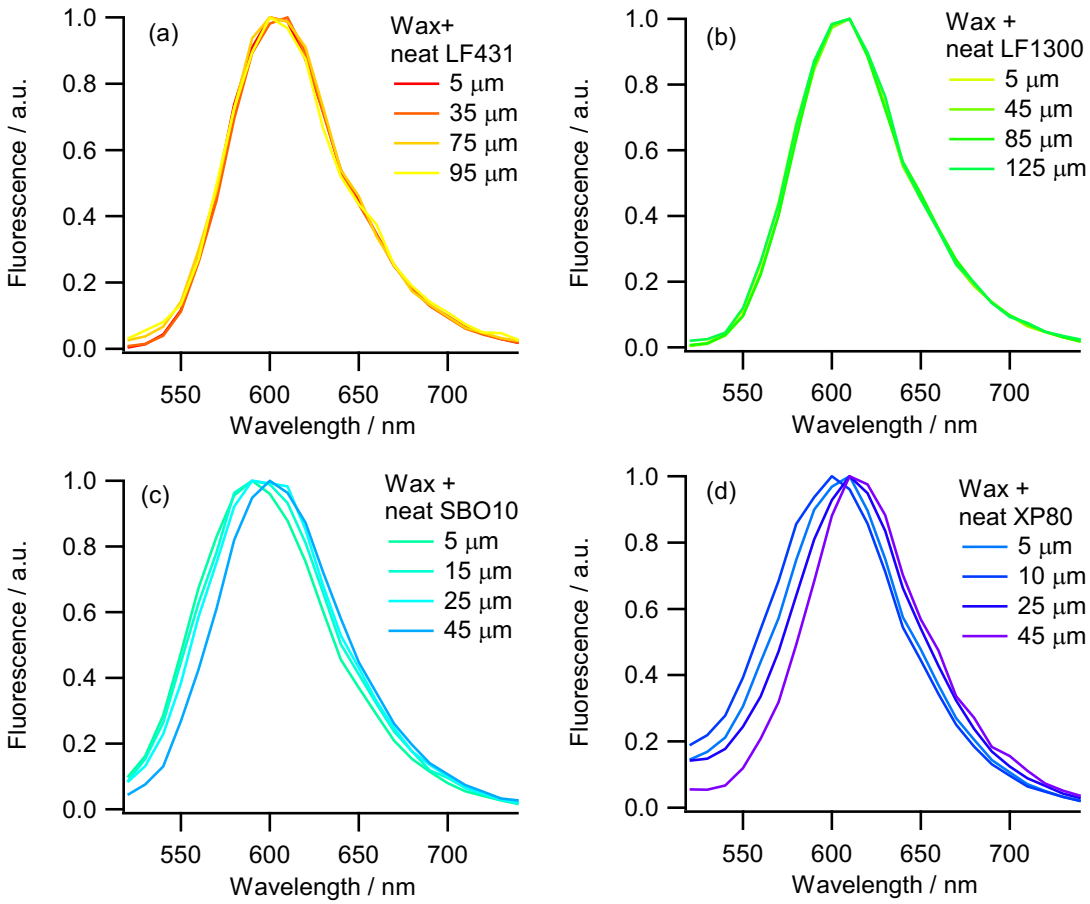

Figure S15. Normalised fluorescence emission spectra recorded for Carnauba Wax samples stained with 330 ppm NR after 72 h of exposure to the neat adjuvants (mentioned in legends): Plurafac® LF431, Plurafac® LF1300, Agnique® SBO10 and Lutensol® XP80. Spectra recorded following 930 nm excitation without wavelength sensitivity correction at different z-positions within the wax layer, see Figure 5c of the main text for the schematic presentation of the experiment. All data were recorded with the same x63 objective and (x1) magnification factor.

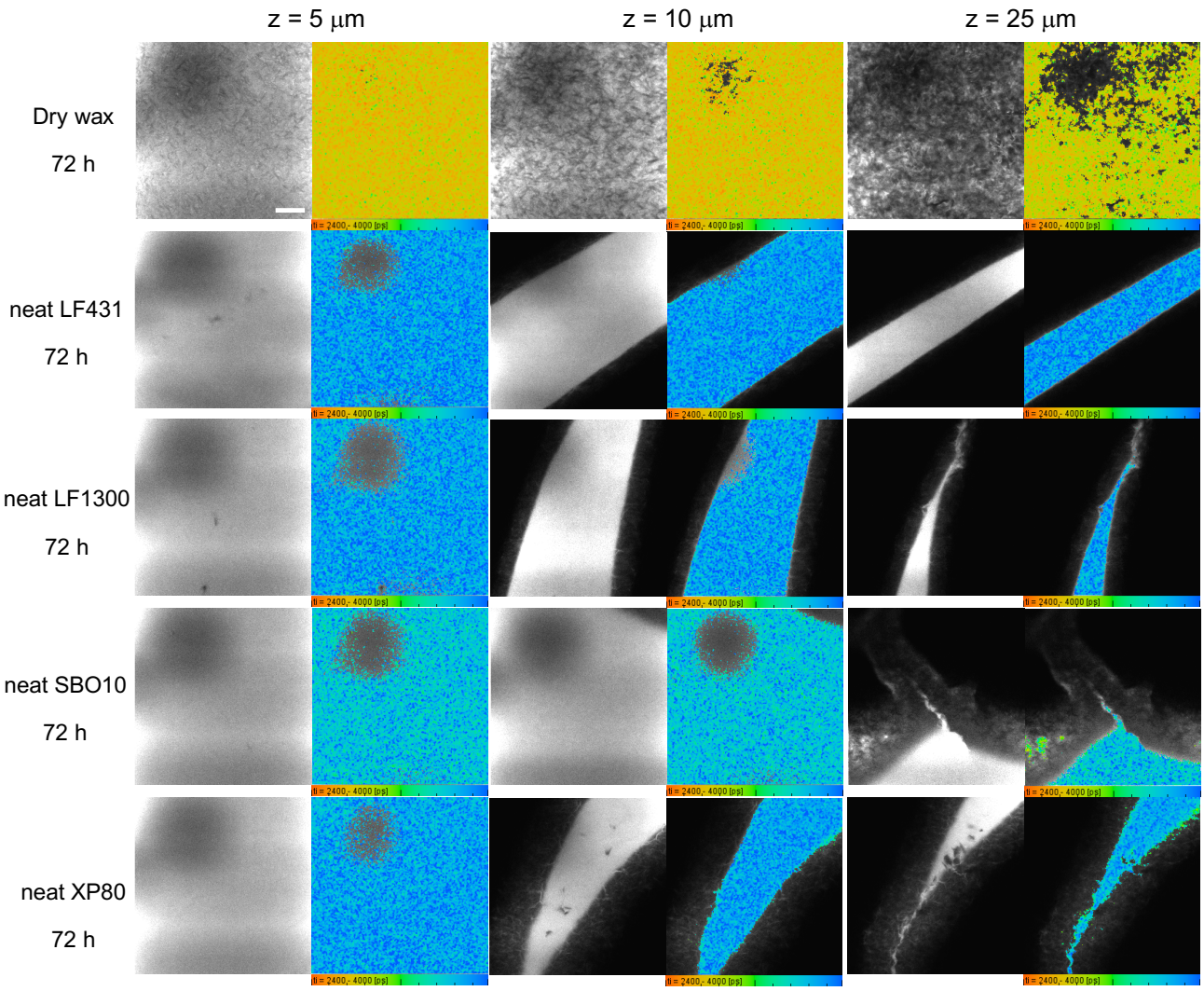

Figure S16. Fluorescence intensity (black and white) and FLIM (coloured) images recorded for Carnauba Wax samples stained with 330 ppm NR after 72 h of exposure to the neat adjuvants (described in the left column): Plurafac® LF431, Plurafac® LF1300, Agnique® SBO10 and Lutensol® XP80. Images recorded following 930 nm excitation and 520-700 nm emission detection at different z-positions within the wax layer, see Figure 5c of the main text for the schematic presentation of the experiment. All data were recorded with the same x63 objective and (x1) magnification factor; the scale bar is 40 μm for all images.

References:

1. Sherin, P.S.; Rueckel, M.; Kuimova, M. Fluorescent Molecular Rotors Quantify an Adjuvant-Induced Softening of Plant Wax. *Chem. Biomed. Imaging*, **2024**, *2*, 453−461. DOI: 10.1021/cbmi.4c00005
2. Dunn, K.W.; Kamocka, M. M.; McDonald, J. H. A practical guide to evaluating colocalization in biological microscopy. *Am. J. Physiol. Cell Physiol.*, **2011**, *300*, C723-C742. DOI: 10.1152/ajpcell.00462.2010
3. Callinan, T. D.; Parks, A. M. The Dielectric Constants and Loss Factors of Some Natural Waxes. *1959 Conference on Electrical Insulation*., **1959**, 45-49. DOI: 10.1109/EIC.1959.7533355
4. Vyšniauskas, A.; López-Duarte, I.; Duchemin, N.; Vu, T. T.; Wu, Y.; Budynina, E. M.; Volkova, Y. A.; Peńa Cabrera, E.; Ramirez-Ornelas, D. E.; Kuimova, M. K. Exploring Viscosity, Polarity and Temperature Sensitivity of BODIPY-based Molecular Rotors. *Phys. Chem. Chem. Phys*., **2017**, *19*, 25252. DOI: 10.1039/c7cp03571c
5. Dutt, G. B.; Doraiswamy, S.; Periasamy, N.; Venkataraman B. Rotational Reorientation Dynamics of Polar Dye Molecular Probes by Picosecond Laser Spectroscopic Technique. *J. Chem. Phys.*, **1990**, *93*, 8498. DOI: 10.1063/1.459288
6. Dutta, A. K.; Kamada, K.; Ohta, K. Spectroscopic Studies of Nile Red in Organic Solvents and Polymers. *J. Photochem. Photobiol. A Chem.*, **1996**, *93*, 57. DOI: 10.1016/1010-6030(95)04140-0
7. Cser, A.; Nagy, K.; Biczók, L. Fluorescence Lifetime of Nile Red as a Probe for the Hydrogen Bonding Strength with its Microenvironment. *Chem. Phys. Lett.*, **2002**, *360*, 473-478. DOI: 10.1016/S0009-2614(02)00784-4
8. Yablon, D.G.; Schilowitz, A.M. Solvatochromism of Nile Red in Nonpolar Solvents. *Applied Spectroscopy*, **2004**, *58*, 843-847. DOI: 10.1366/0003702041389328.
9. Kamlet, M. J.; Abboud, J-L. M.; Abraham, M. H.; Taft, R.W. Linear Solvation Relationships. 23. A Comprehensive Collection of the Solvatochromic Parameters, π^*,α and β, and Some Methods for Simplifying the Generalized Solvatochromic Equation, *J. Org. Chem.*, **1983**, *48*, 2877. DOI: 10.1021/jo00165a018
10. Maillard, J.; Klehs, K.; Rumble, C.; Vauthey, E.; Heilemann M.; Fürstenberg, A. Universal Quenching of Common Fluorescent Probes by Water and Alcohols. *Chem. Sci.*, **2021**, *12*, 1352–1362. DOI: 10.1039/d0sc05431c
11. Sherin, P.S.; Grilj, J.; Tsentalovich, Yu.P.; Vauthey, E. Ultrafast Excited-State Dynamics of Kynurenine, a UV Filter of the Human Eye, *J. Phys. Chem. B*, **2009**, *113*, 4953. DOI: 10.1021/jp900541b.
12. Fita, P.; Fedoseeva M.; Vauthey, E. Ultrafast Excited-State Dynamics of Eosin B: A Potential Probe of the Hydrogen-Bonding Properties of the Environment. *J. Phys. Chem. A*, **2011**, *115*, 2465. DOI: 10.1021/jp110849x

13. Dereka B.; Vauthey, E. Direct Local Solvent Probing by Transient Infrared Spectroscopy Reveals the Mechanism of Hydrogen-Bond Induced Nonradiative Deactivation *Chem. Sci.*, **2017**, *8*, 5057. DOI: 10.1039/C7SC00437K

14. Yeats, T. H.; Rose, J. K. C. The Formation and Function of Plant Cuticles. *Plant Physiol.*, **2013**, *163*, 5. DOI: 10.1104/pp.113.222737